Journal of Rock Mechanics and Geotechnical Engineering 16 (2024) 909–923

Contents lists available at ScienceDirect

Journal of Rock Mechanics and Geotechnical Engineering

journal homepage: www.jrmge.cn

Full Length Article

A method to predict rockburst using temporal trend test and its application

Yarong Xue [a], Zhenlei Li [a], Dazhao Song [a,*], Xueqiu He [a,b], Honglei Wang [a], Chao Zhou [a], Jianqiang Chen [c], Aleksei Sobolev [d]

[a] School of Civil and Resources Engineering, University of Science and Technology Beijing, Beijing, 100083, China
[b] Zhong-an Academy of Safety Engineering, Beijing, 100083, China
[c] China Energy Group Xinjiang Energy Co., Ltd, Urumqi, 830027, China
[d] Khabarovsk Federal Research Center of the Far Eastern Branch of the Russian Academy of Sciences (KhFRC FEB RAS), 51 Turgenev Street, Khabarovsk, 680000, Russia

ARTICLE INFO

Article history:
Received 27 December 2022
Received in revised form
15 May 2023
Accepted 9 July 2023
Available online 29 September 2023

Keywords:
Rockburst
Microseismicity
Early warning
Mann-Kendall trend test
Confusion matrix
Multi-indices fusion

ABSTRACT

Rockbursts have become a significant hazard in underground mining, underscoring the need for a robust early warning model to ensure safety management. This study presents a novel approach for rockburst prediction, integrating the Mann-Kendall trend test (MKT) and multi-indices fusion to enable real-time and quantitative assessment of rockburst hazards. The methodology employed in this study involves the development of a comprehensive precursory index library for rockbursts. The MKT is then applied to analyze the real-time trend of each index, with adherence to rockburst characterization laws serving as the warning criterion. By employing a confusion matrix, the warning effectiveness of each index is assessed, enabling index preference determination. Ultimately, the integrated rockburst hazard index Q is derived through data fusion. The results demonstrate that the proposed model achieves a warning effectiveness of 0.563 for Q, surpassing the performance of any individual index. Moreover, the model's adaptability and scalability are enhanced through periodic updates driven by actual field monitoring data, making it suitable for complex underground working environments. By providing an efficient and accurate basis for decision-making, the proposed model holds great potential for the prevention and control of rockbursts. It offers a valuable tool for enhancing safety measures in underground mining operations.

1. Introduction

Rockburst, which is considered one of the most severe dynamic disasters in coal mines, refers to the sudden and forceful ejection of coal and rock masses caused by the accumulation of elastic deformation energy internal. It often leads to casualties and substantial property damage (Cai et al., 2020; Xue et al., 2021; Zhu et al., 2016, 2018). With the continuous expansion of coal mining into deeper areas, the coal seam structure of the stope and the surrounding rock storage conditions around the roadway have become increasingly complex. Consequently, the internal dynamic response characteristics of coal and rock masses have become more intricate (He et al., 2020). As a result, the frequency of rockburst hazards has risen sharply, posing significant threats to the safety of individuals working in mines and their properties.

In an effort to prevent and control rockburst disasters, the microseismic (MS) monitoring system has been widely adopted in underground mines, proving to be a powerful tool for rockburst prediction. Lu et al. (2015) investigated the evolutionary patterns of multi-parameter precursory characteristics before and after rockburst events. Cao et al. (2016) conducted a qualitative analysis of the evolution of microseismicity leading up to a catastrophic rockburst. Their study concluded that abnormal clustering of seismic sources, abnormal variations in daily total energy release, and event counts could be considered precursors to rockburst incidents. Yu et al. (2016) indicated that the daily maximum MS energy could be used to estimate rockburst intensity. Tang et al. (2018) proposed that the spatial and temporal concentration of MS events,

* Corresponding author.
E-mail address: songdz@ustb.edu.cn (D. Song).
Peer review under responsibility of Institute of Rock and Soil Mechanics, Chinese Academy of Sciences.

https://doi.org/10.1016/j.jrmge.2023.07.017

along with a decrease in the *b*-value, can be regarded as precursors to the instability of the surrounding rock. He et al. (2019) conducted a study on the variations in MS and acoustic emission monitoring data prior to rockburst events in steeply inclined and extremely thick coal seams. They established the energy deviation value and total deviation high-value indicators as precursory warnings for rockburst. Li et al. (2021) observed a decreasing trend in MS events prior to rockbursts, accompanied by a "quiet period," while electromagnetic radiation intensity increased and reached a maximum before rockbursts. Zhang et al. (2021) proposed that peak particle velocity could serve as an early warning index for rockburst, emphasizing the need to consider this indicator alongside post-processing indicators such as event energy. Additionally, various indicators such as fractal dimension, *b*-value, apparent cumulative apparent volume, the energy index, cumulative released energy, and the *Es/Ep* value of MS events have been analyzed in relation to rockburst events. These analyses provide valuable insights for rockburst prediction (Feng et al., 2016; Mondal and Roy, 2019; Xie and Pariseau, 1993; Xue et al., 2020).

However, due to the complexity of rockburst occurrence mechanisms, the use of different warning indicators can lead to varied warning results for the same event. This is because these indicators reflect the evolution of rockburst precursors based on different principles. Consequently, assessing the actual hazard state can pose challenges for the mine personnel. Consequently, there have been notable efforts to develop a multi-indices rockburst early warning model to improve the accuracy of predictions. Cai et al. (2014) developed a multidimensional index system that incorporates MS information. They combined the comprehensive anomaly index method with the *R*-value method to provide a quantitatively description of the real-time rockburst hazard status. Liu et al. (2016) introduced a methodology for dynamic risk assessment and management of rockbursts in drill and blast tunnels. The approach utilizes quantitative MS indices to evaluate the probability of rockburst occurrence. Cai et al. (2018) proposed a fuzzy comprehensive rockburst risk evaluation model. The model incorporates components such as the Gaussian shape membership function, the confusion matrix and the maximum membership degree principle. Dou et al. (2018) utilized the *R*-value scoring method to determine the weights and estimate the critical values of various MS indicators, such as bursting strain energy, time-space-magnitude independent information, and time-space-magnitude compound information. The study demonstrated that their comprehensive index effectively quantifies the pre-warning of rockburst risk. Cao et al. (2020) developed a probabilistic forecasting methodology for rockburst hazard at Coal Mine Velenje. Their approach integrated data-driven techniques with a physics-based framework, utilizing MS monitoring data in conjunction with concurrent face advance records. The study achieved satisfactory results, highlighting the effectiveness of their methodology in rockburst hazard assessment. In a study by Feng et al. (2015), a microseismicity-based rockburst warning method was proposed. This method utilized real-time microseismic data and a rockburst warning formula. The formula included a rockburst database, selection of typical rockburst cases, functional relationships between microseismicity and rockbursts, optimal weighting coefficients, and dynamic updating. The method was successfully applied to rockburst warning in deep tunnels at the Jinping II hydropower project. Yin et al. (2021) proposed an integrated CNN-Adam-BO algorithm based on microseismic monitoring data for real-time prediction of rockburst intensity. Cao et al. (2022) presented a knowledge and data fusion-driven deep neural network called FDNet for coal burst prediction. The FDNet used the existing mine seismic model to extract explicit features and employed deep learning to automatically extract implicit features from mine microseismic data. This approach provided new insights in coal burst prediction. In addition, decision tree (Wang, 2021; Zhao et al., 2021), support vector machine (Ji et al., 2020; Jin et al., 2022), neural network (Feng et al., 2019), and other algorithms have also been used to establish new multi-indices fusion early warning models for rockburst.

Although significant advancements have been made in rockburst early warning models, the currently available single-indicator or multi-indicator warning methods mostly rely on threshold values to determine whether an alarm is triggered. However, the occurrence of rockburst is a complex nonlinear process with mechanisms that are not fully understood. This lack of understanding has created a challenge in improving the accuracy of existing rockburst warning methods. On-site empirical evidence indicates that there are anomalous patterns preceding rockburst incidents. However, these patterns are often less considered in existing warning methods. Therefore, to enhance the accuracy of warnings, it is crucial to establish a rockburst early warning model that incorporates multidimensional warning indicators and captures real-time changes in these indicators.

To address the aforementioned limitations, this paper proposes a multi-indices fusion rockburst early warning model based on the Mann-Kendall trend test method (MKT). The model aims to improve the rockburst early warning precision by incorporating multiple indicators and utilizing MKT for trend analysis. The model initiates by applying MKT to capture the temporal changes of multidimensional rockburst precursory indices. It evaluates whether the changing trends conform to the characterization law of rockburst precursors, forming the foundation for early warning. The model continuously updates and selects the indices by utilizing the confusion matrix to reevaluate the early warning effectiveness of each index. This process ensures that the most effective indices are chosen for optimal performance in predicting rockburst events. The effectiveness of early warnings serves as the data fusion weight, leading to a quantified comprehensive rockburst hazard evaluation index. The proposed model has demonstrated successful applications at Kuangou Coal Mine in China, providing a timely and accurate decision-making tool for the prevention and control of underground rockburst incidents.

2. Principles and methodology

Pu et al. (2019, 2020) have found that rockburst is a complex nonlinear process; that is, there is a degree of uncertainty in the occurrence of precursor anomalies of rockbursts. This uncertainty arises from the incomplete understanding of the mechanism and the difficulty in specifying relevant measurement parameters during the rockburst evolution. Nevertheless, rockburst is fundamentally the result of failure stress in coal and rock masses, leading to the formation of large internal cracks and energy release. Extensive research has identified various precursory indices that reflect the process of fissures initiation, propagation, convergence, and connection into macro-fractures in coal and rock masses. The abnormal change trend of each precursory index before rockburst can be regarded as a danger signal and has achieved good application results in infield practice. However, the complex geological environment and mining conditions in each mine give rise to unique characteristics for the application of individual indices in different regions. To enhance the accuracy of rockburst prediction, this paper proposes a multi-indices fusion rockburst early warning model based on the MKT.

2.1. Overview of the multi-indices fusion rockburst early warning model

As illustrated in Fig. 1, the proposed model begins by collecting real-time monitoring data from the online rockburst monitoring system and then uses a certain length of the time window and sliding step to calculate the multidimensional rockburst precursory indices, which reflect the rockburst development process information. The model utilizes MKT to determine the trend of each index, ensuring adherence to the characterization law of rockburst precursors for early warning. The effectiveness of each index is evaluated and ranked using the confusion matrix. Selected indices with high effectiveness are combined to form the integrated rockburst hazard index *Q*. *Q* is categorized into four levels of rockburst risk: no risk, weak risk, medium risk, and high risk, corresponding to specific ranges. More details about the development of the early warning model can be found in the following section.

2.2. Details of the multi-indices fusion rockburst early warning model

2.2.1. Pre-processing of real-time monitoring data

Currently, online monitoring systems for underground dynamic disasters, such as MS, electromagnetic radiation, and acoustic emission, are widely used. These systems capture real-time information on the energy release of coal-rock mass breakage, seismic source location, roof pressure, and other parameters, providing insights into the evolution of coal-rock dynamic hazards. However, the data obtained from these monitoring systems often show irregular time intervals, making it challenging to perform data mining and analysis. To address this challenge, it is necessary to standardize the data obtained from different sources by structuring them with consistent dimensional granularity and attributes.

By dividing the original monitoring data into fixed-length time windows and calculating the feature of each sample within the windows, it is possible to transform irregular time series into regular time series and obtain the trends of the features. This process is illustrated in Fig. 2. Firstly, a sliding time window of length Δt is defined, and the monitoring data time series is divided into n sets of data, each with a length Δt and corresponding to the end moments the time window. The data set for the moment T_i is denoted as $\boldsymbol{X}_i$ $[x_1, x_2, x_3, \ldots, x_k]$ $(k \leq t, 0 < i \leq n)$. The features of all samples in $\boldsymbol{X}_i$ are calculated and arranged in order, resulting in a transformed regular time series. The interval of the transformed time series corresponds to the sliding step size of the time window. The size of the sliding step determines the granularity of the data, and the sliding step size needs to be smaller than the time window length to ensure that no data is omitted.

2.2.2. Trend determination of precursory indices

Extracting meaningful precursory indices from original underground monitoring data is an effective approach for disaster prevention and control in coal-rock dynamic environments. Various precursory indices have been widely utilized, including the *b* value (Gutenberg, 1956), total fault area $A(t)$ (Lu et al., 2015), lack of seismic M_m (Utsu et al., 1995), energy deviation D_E (He et al., 2019), among others. These indices often exhibit a continuous trend of increase or decrease before the occurrence of disasters like rockbursts, enabling timely hazard level assessment. However, the range of each index varies significantly under complex mining conditions and geological environments. Consequently, the conventional approach of using a single critical value lacks scalability, as it varies with specific mine conditions. This limitation necessitates a more effective time series trend test method for practical application of precursory indices, as relying solely on human experience to identify abnormal trends hampers the utilization efficiency of these indices.

We performed MKT to determine the monotonic trends in the time series of precursory indices. MKT is rank-based and nonparametric, which means it does not rely on specific data distribution and emphasizes the relative order of magnitude rather than the actual data values. Furthermore, MKT is capable of handling extreme values, making it highly suitable for analyzing underground mine monitoring data. The MKT can be defined as

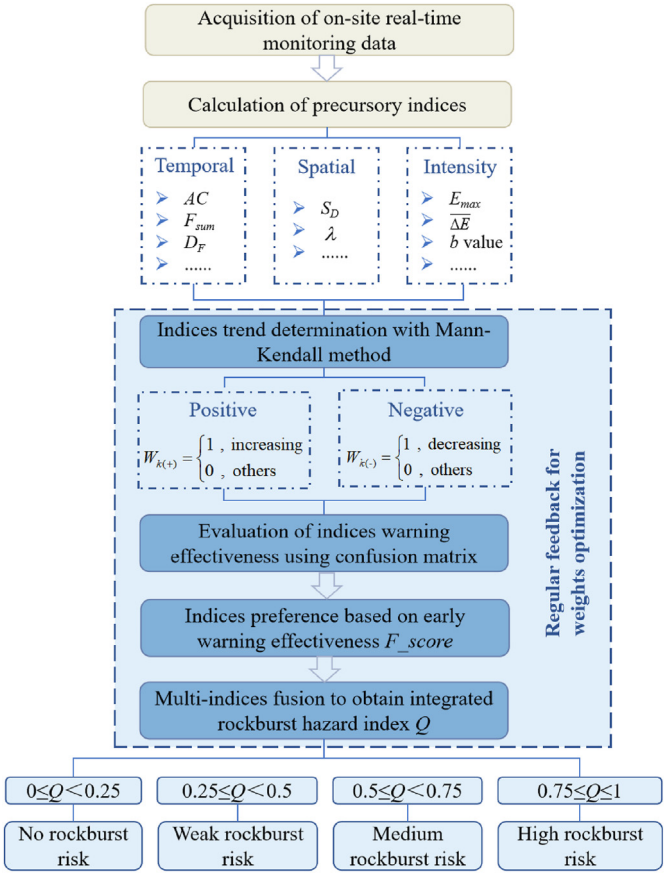

Fig. 1. Multi-indices fusion rockburst early warning model.

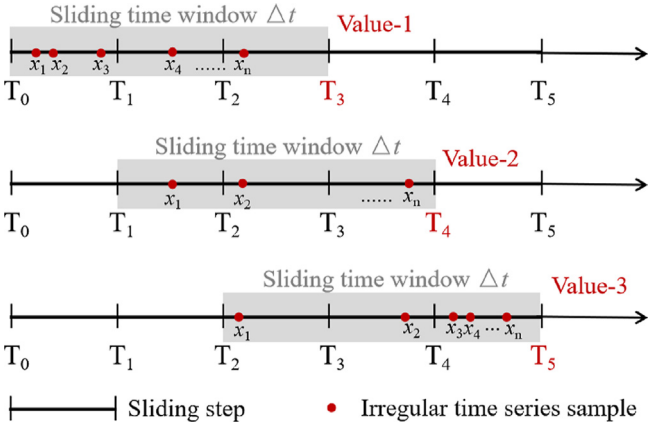

Fig. 2. Pre-processing of irregular monitoring data (Cai et al., 2018).

$$S = \sum_{k=1}^{n-1}\sum_{j=k+1}^{n}\mathrm{sgn}(x_j - x_k) \tag{1}$$

$$\mathrm{sgn}(x_j - x_k) = \begin{cases} +1((x_j - x_k) > 0) \\ 0((x_j - x_k) = 0) \\ -1((x_j - x_k) < 0) \end{cases} \tag{2}$$

where n presents the length of dataset $\boldsymbol{X}_i$ [x_1, x_2, x_3, …, x_n], x_k corresponding to the rank for the kth observations ($k = 1, 2, 3, \ldots, n-1$), and x_j represents the rank for the jth observations ($j = k+1, 2, 3, \ldots, n$).

According to Mann and Kendall (Mann, 1945; Kendall, 1948), when the value of n is greater than or equal to 10, the statistic S follows an approximate normal distribution with the following mean and variance:

$$E(S) = 0 \tag{3}$$

$$VAR(S) = \frac{1}{18}\left[n(n-1)(2n+5) - \sum_{p=1}^{g} t_p(t_p-1)(2t_p+5)\right] \tag{4}$$

where n represents the length of dataset $\boldsymbol{X}_i$ [x_1, x_2, x_3, …, x_n], g represents the number of these equal trend values or groups, and t_p represents the number of data values in the pth group.

The Kendall standardized test statistics Z is calculated as

$$Z = \begin{cases} \dfrac{S-1}{\sqrt{VAR(S)}}(S > 0) \\ 0(S = 0) \\ \dfrac{S+1}{\sqrt{VAR(S)}}(S < 0) \end{cases} \tag{5}$$

If the calculated value of Z is greater than zero and passes the significance test (with a significance level of $\alpha = 0.05$ and $Z = \pm 1.96$), it indicates an increasing trend in the data. Conversely, if the calculated value of Z is less than zero, it suggests a decreasing trend in the data. However, if Z does not pass the significance test, it implies that the data does not exhibit an obvious change trend. This approach allows for the statistical analysis of trend behavior in the data, providing valuable insights into the temporal variations of rockburst-related indicators.

2.2.3. Evaluation of early warning effectiveness and preference of indices

Numerous studies have focused on rockburst precursory indices, offering valuable insights into the evolution of rockbursts from multiple perspectives such as time, space, and intensity. These indices exhibit different response characterization laws influenced by various contributing factors. Consequently, the evaluation and selection of precursory indices play a crucial role in determining early warning levels during field applications. To enhance decision-making efficiency for underground personnel, it is important to choose appropriate indices and assign them appropriate weights. In this study, the effectiveness of each precursory index is evaluated and optimized using *F_score* in Table 1. The matrix includes true positive (TP) and true negative (TN) values, representing correct warnings, and false positive (FP) and false negative (FN) values, representing false and missed warnings. Initially, actual monitoring data and records of high-energy tremors and rockburst events are used to calculate and rank the *F_score* for each index in the precursory database. Indices with high *F_scores* are selected as the foundation for the model. The indices are periodically re-evaluated and selected to ensure their efficiency in assisting the model's early warning decisions. Further details can be found in Fig. 1.

2.2.4. Multi-indices fusion and rockburst risk classification

Integrating various multidimensional coal-rock dynamic disaster early warning indices that consider temporal, spatial, and intensity aspects is crucial for creating a unified and quantitative real-time warning system with consistent criteria and thresholds. By applying the comprehensive anomaly index method (Cai et al., 2014), the integrated rockburst hazard index Q is constructed, and its calculation method is shown in Eq. (6):

$$Q = \sum_{k=1}^{n}\left(\frac{e - e^{1-W_{k(+/-)}}}{e-1}\frac{F_k}{\sum_{k=1}^{n} F_k}\right) \tag{6}$$

where n represents the total number of preferred precursory indices, F_k represents the *F_score*, which reflects the early warning effectiveness of the k-th indicator. $W_{k(\pm)}$ represents the anomaly membership of the k-th index, and they range from 0 to 1. The calculation of $W_{k(\pm)}$ can be performed using the following method.

For the positive precursory index, using MKT to determine its trend in the previous period and get

$$W_{k(+)} = \begin{cases} 1 \ (\text{increasing}) \\ 0 \ (\text{others}) \end{cases} \tag{7}$$

For the negative precursory index, the same reasoning yields

$$W_{k(-)} = \begin{cases} 1 \ (\text{decreasing}) \\ 0 \ (\text{others}) \end{cases} \tag{8}$$

Based on theoretical analysis and numerous field experiments, the coal-rock dynamic hazard level can be categorized into four levels (Dou and He, 2007). These hazard levels align with the classifications specified in the "Rules for Prevention and Control of Coal Mine Rockburst, China." The corresponding hazard levels are presented in Table 2.

Table 1
Calculation of the confusion matrix and early warning effectiveness (Fawcett, 2006).

Total population		Actual condition		$F\_score = \frac{2 \cdot Recall \cdot Precision}{Recall + Precision}$
		Rockburst or high energy tremor (Positive)	No rockburst or high energy tremor (Negative)	
Early warning condition	Rockburst or high energy tremor (Positive)	True Positive (TP)	False Positive (FP)	*Precision* = TP/(TP + FP)
	No rockburst or high energy tremor (Negative)	False Negative (FN)	True Negative (TN)	*Negative precision* = TN/(TN + FN)
		Recall = TP/(TP + FN)	*Specificity* = TN/(TN + FP)	*Accuracy* = (TP + TN)/(TP + TN + FP + FN)

Table 2
Classification standard for coal-rock dynamic hazards.

Integrated rockburst hazard index Q	Levels of rockburst risk	State of rockburst risk
$0 \leq Q < 0.25$	I	No rockburst risk
$0.25 \leq Q < 0.5$	II	Weak rockburst risk
$0.5 \leq Q < 0.75$	III	Medium rockburst risk
$0.75 \leq Q \leq 1$	IV	Strong rockburst risk

3. Case study

3.1. Engineering description and rockburst contributing factor analysis

Kuangou Coal Mine (KCM) is situated in Urumqi, Xinjiang Province, China. The mine has six mineable coal seams ranging from shallow to deep: B4-2 (mined out), B4-1 (mined out), B3, B2 (under mining), B1, and B0. Currently, mining activities are mainly concentrated in the I010203 working face of the B2 coal seam, and the general layout and stratigraphic structure diagram of KCM are shown in Figs. 3 and 4. In Fig. 3, the black line represents the working face and roadway in the B2 seam, while the blue line represents the working face and roadway in the B4-1 seam. The I010203 working face has an inclination width of 192 m and a strike length of 1,469 m. It employs the fully mechanized caving mining method, with a coal cutting thickness of 3.2 m and a roof coal release thickness of 6.3 m. The average burial depth is approximately 350 m. The working face is situated on the west side of the safety coal block, with a 15 m section pillar reserved between its north side and the I010201 goaf of the same coal seam. Moreover, the I010403 and I010405 goafs are situated around 70 m above the I010203 working face in the B4-1 coal seam, forming a "knife-handle" boundary. The B1 coal seam, which is yet to be mined, lies approximately 30 m below the B2 coal seam. Within the working face, there is a significant fault labeled F2-1, which has an inclination of 60° and a fault displacement of 2.9–6.8 m. According to the test, the average duration of dynamic fracture *DT* of B2 coal seam at different locations is 250.33ms, the elastic strain energy index W_{ET} is 3.43, the bursting energy index K_E is 2.79, the uniaxial compressive strength R_C is 26.34 MPa, according to the Methods for Test, Monitoring and Prevention of Rockburst (GB/T 25217.2–2010), B2 coal seam has weak bursting liability. In the same way, the roof of B2 coal seam has strong bursting liability and the floor has weak bursting liability.

KCM is equipped with the ARAMIS M/E MS monitoring system. The MS sensors have a sampling frequency of 500 Hz and a sensitivity of 110 Vs/m ± 10%. These sensors are capable of monitoring low-frequency high-energy MS events with an energy threshold of 100 J and a frequency range of 0–150 Hz. The positioning accuracy of the sensors is ±20 m in the *X* and *Y* directions and ±50 m in the *Z* direction. Based on the geological conditions and characteristics of the surrounding rocks at location I010203, 2 MS sensors were arranged in the haulage roadway of the working face with a spacing of 150 m, marked as S2 and T3; 1 MS sensor was arranged in the craft lane, marked as T16; 2 MS sensors were arranged in the ventilation roadway with a spacing of 150 m, marked as T10 and T11 (see Fig. 3). To ensure that the working face remains within the detection range of the MS sensors, a specific adjustment is made when the sensors are located less than 50 m away from the working face. In such cases, the sensors are shifted 300 m ahead of the working face. This adjustment ensures that the working face remains within the coverage area of the MS sensors for effective monitoring. (Please refer to Khan et al., 2022 for more details about the MS system). From February 1, 2018, to January 31, 2019, a total of 15 rockburst events have occurred at the I010203 working face during this period, and the location of each event source is shown in Fig. 5, and the information is shown in Table 3, which shows that:

(1) Rockburst events occur at varying focal locations, with the majority concentrated within the range of 0–365 m from the leading working face. The density of focal locations is high both before and after the fault location, with a significant number of events occurring in the haulage roadway and

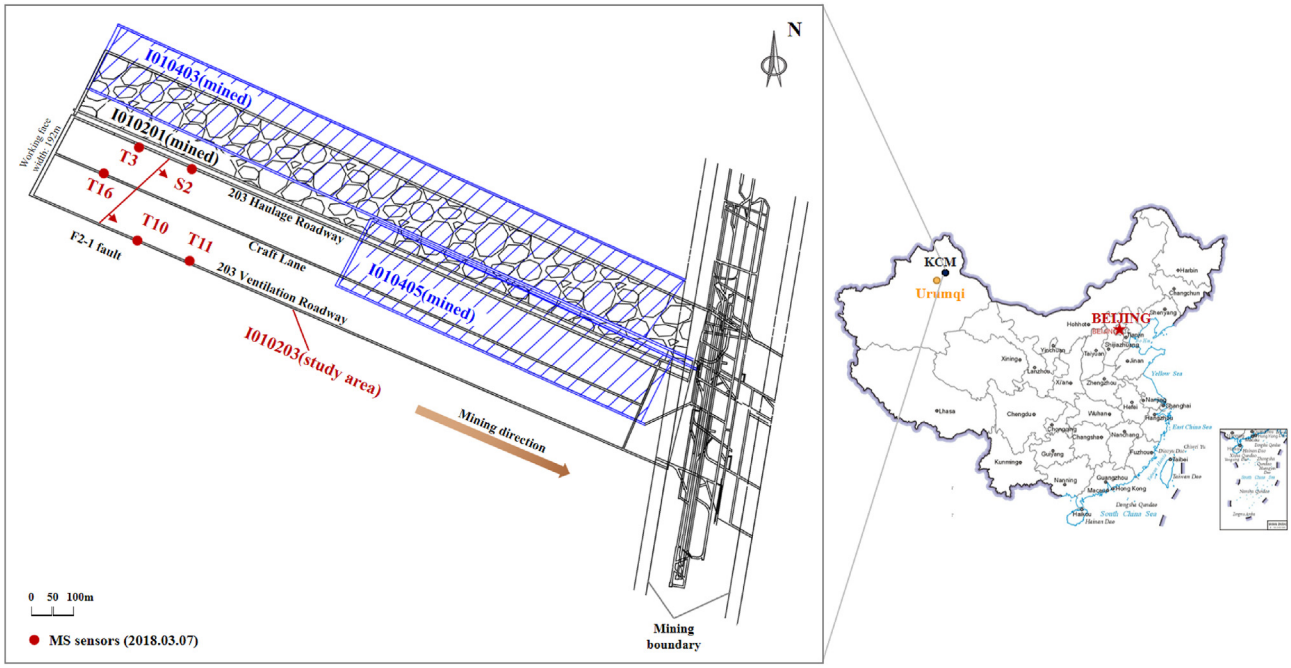

Fig. 3. Geological condition of KCM and the layout of MS monitoring system installed until March 7, 2018.

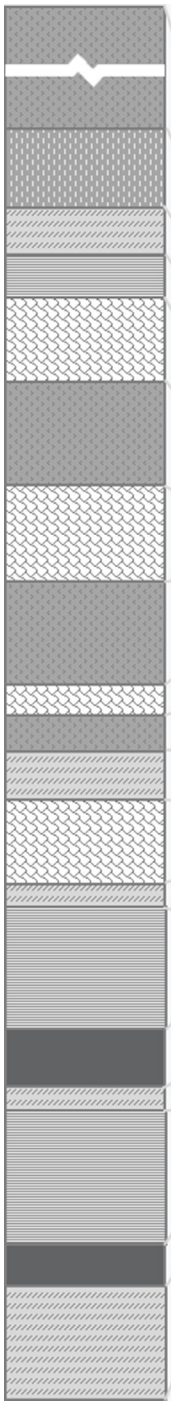

Lithology	Thickness(m)	Key stratum position	Description
siltstone	166		Gray, dark gray, locally black carbonaceous mudstone
gravelly sandstone	13	Inferior key strata	Grayish-white, dense, hard
mudstone	8		Gray, dark gray, locally black carbonaceous mudstone
fine-grained sandstone	7		Grayish-white, dense, hard
medium-grained sandstone	14		Black, predominantly laminated with dark shallow coal
siltstone	17		Contains white mica flakes, predominantly quartz and feldspar, relatively hard
medium-grained sandstone	16		Gray, dark gray, locally black carbonaceous mudstone
siltstone	17	Main key strata	Contains white mica flakes, predominantly quartz and feldspar, relatively hard
medium-grained sandstone	5		Gray, dark gray, locally black carbonaceous mudstone
siltstone	6	Inferior key strata	Contains white mica flakes, predominantly quartz and feldspar, relatively hard
mudstone	8		Black, predominantly laminated with dark shallow coal
medium-grained sandstone	14	Main key strata	Gray, dark gray, locally black carbonaceous mudstone
mudstone	4		Contains white mica flakes, predominantly quartz and feldspar, relatively hard
fine-grained sandstone	20		Gray, dark gray, locally black carbonaceous mudstone
B2 coal	9.5		**Main mining seam, in which working faces I010203 and I010201 are located.** Black, predominantly laminated with dark shallow coal
mudstone	4		Grayish-white, dense, hard
fine-grained sandstone	22		Gray, dark gray, locally black carbonaceous mudstone
B1 coal	7		Black, predominantly laminated with dark shallow coal
mudstone	18.7		Contains white mica flakes, predominantly quartz and feldspar

Fig. 4. Schematic diagram of stratigraphic structure.

some in the surrounding rock near the ventilation roadway. The range of rockburst events typically falls within 100–550 m from the working face. This indicates that the highest rockburst risk is observed within the 100–550 m range from the cutting hole.

(2) The majority of rockburst sources are located in the coal seam and roof in the middle and lower sections of the working face. They also occur in the roof and section coal pillar in the lateral goaf. These areas are identified as the main elastic energy concentration areas, and the event density of the roof in the vertical direction is significantly higher than that of the floor (11 out of 15 times). The breaking of the hard roof is the main inducing factor of the rockburst of KCM.

The analysis results show that the hard roof breakage at I010203 is the main inducing factor of rockburst events, and rockbursts are often preceded by high-energy tremors (energy $>10^6$ J), which are a direct cause of rockbursts as a dynamic load disturbance (Manouchehrian and Cai, 2017; Wang et al., 2018). Based on this, the MS data collected by the MS sensors at the I010203 working face are used as the basis for extracting the precursor indices of

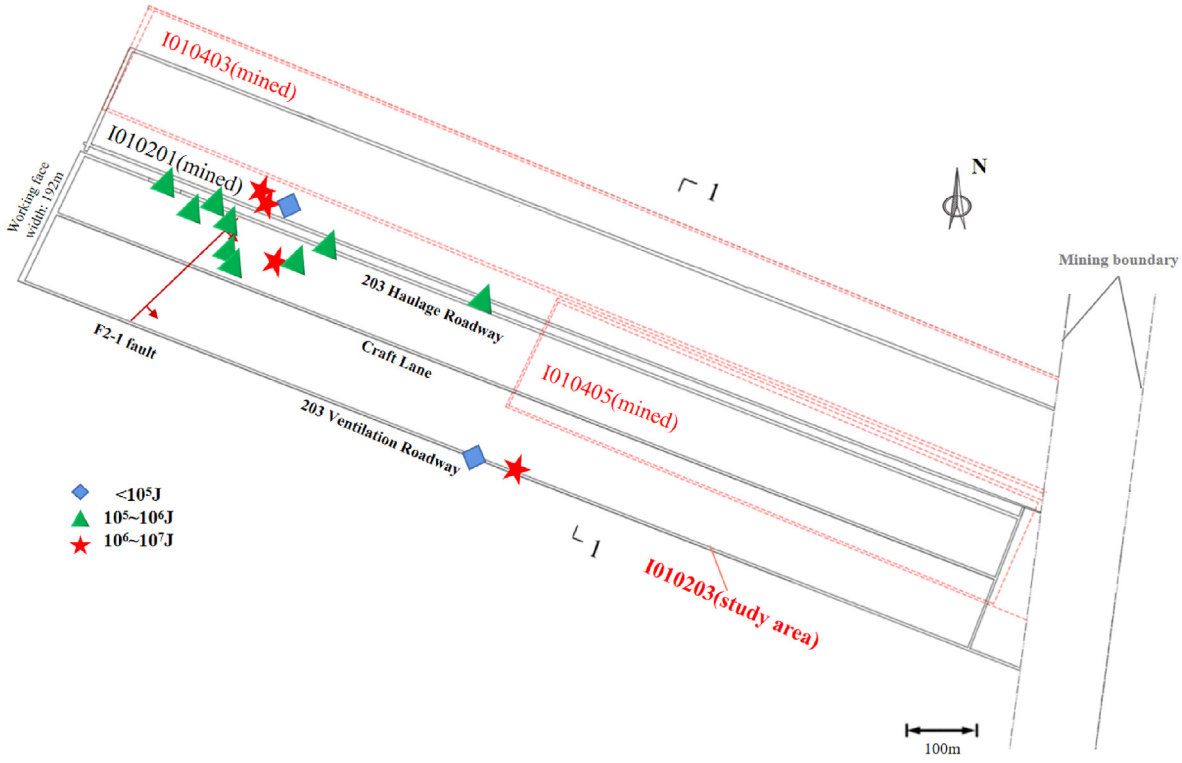

(a) Plane figure.

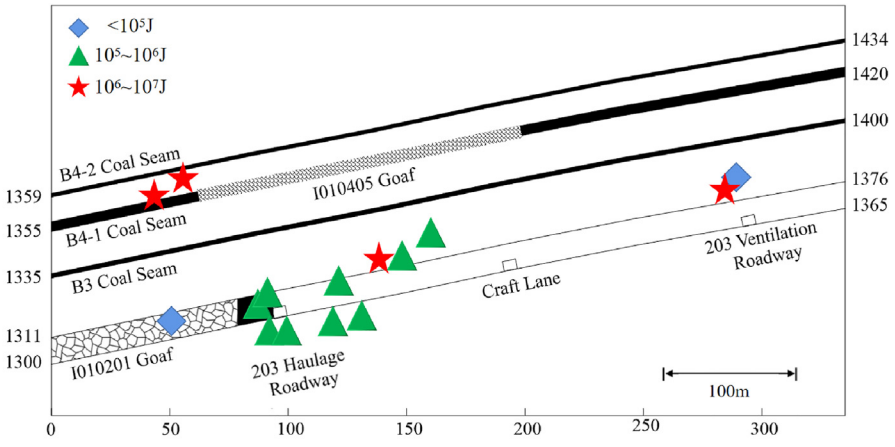

(b) Sectional figure (1-1).

Fig. 5. Source location diagram of each rockburst events.

coal-rock dynamic hazards to predict the occurrence of high-energy tremors. These indices enable the prediction of high-energy tremors and subsequently facilitate the monitoring and warning of rockburst hazards.

3.2. Rockburst precursory indices

The effective utilization of MKT for monitoring and early warning of rockbursts relies on the availability of accurate precursory indices that possess clear physical significance. Numerous researchers (Cai et al., 2014, 2018; He et al., 2019, 2021; Liu et al., 2019; Lu et al., 2015; Ma et al., 2019; Qin et al., 2019; Xu et al., 2017; Yu et al., 2017) have proposed multidimensional precursory indices based on the "temporal-spatial-intensity" framework and these indices can effectively capture the evolving patterns preceding rockburst events, and their practical application in mining has yielded positive results. Therefore, KCM adopts a library of 18 precursory indices to monitor and predict rockburst events, as shown in Fig. 6. For detailed descriptions each warning index, please refer to Xue et al. (2023).

From February 1, 2018, to January 31, 2019, the I010203 working face experienced a series of rockburst events, making it an ideal case study site. During this period, a total of 30065 MS events (Except September 24 to October 19, 2018, with no data recorded because of working face closure) and 15 rockburst events (see Table 3). A time window of 15-d and a sliding step of 1-d are employed to calculate of the actual values for each index, and its time-sequence evolution graphs are shown in Fig. 7.

Table 3
Overview of each rockburst event.

No.	Date	The distance ahead of working face (m)	Energy (J)	Main damage
1	2018.03.07	60	3.1×10^5	Local collapse on the lower wall.
2	2018.03.08	210	9.7×10^6	The floor bulges about 20 cm, and the local top coal sinks about 30 cm
3	2018.03.26	105	5.2×10^5	Local collapse on the south wall
4	2018.04.08	200	4.7×10^5	Slight slag dropping in the affected area
5	2018.04.14	70	1.7×10^5	Slight slag dropping in the affected area
6	2018.04.16	118	3.3×10^5	The roof collapses locally, the roadway floor bulges about 30 cm
7	2018.04.27	90	2.1×10^4	The roof collapses locally, the roadway floor bulges about 30 cm
8	2018.05.07	365	3.2×10^6	The roadway floor bulges 20 −40 cm, and three anchor bolt supporting plates fall
9	2018.05.20	110	9.5×10^5	
10	2018.06.13	132	1.4×10^5	Strong tremors at the working face
11	2018.06.25	84	4.0×10^6	One support sinks by 17 cm, the width of the roadway is deformed by 10 cm
12	2018.07.23	116.9	4.6×10^6	The width of the roadway is deformed by 10 cm
13	2018.09.16	19	8.5×10^5	Six bolts fail at the transfer machine; Roof subsidence in 1000 −1030m area of haulage roadway is 20–30 cm, and the lower wall sinks about 20 cm
14	2019.01.22	184	5.1×10^4	The roof of the haulage roadway is broken, and the wall protrudes by 15 cm
15	2019.01.23	254	5.7×10^5	The roof at the head of the transfer machine is slightly broken

Prior to the occurrence of a rockburst, each precursory index shows abnormal changes, characterized by a continuous increase or decrease. The values of these indices fluctuate within a range of high or low values until the rockburst event eventually takes place. For example, $A(t)$ (see Fig. 7l) demonstrates a rapid increase in the period leading up to a rockburst event, exhibiting a notable high-value anomaly, indicating that the internal crack propagation degree of coal and rock mass increases rapidly, the number of large cracks increases, and the fracture of coal and rock mass intensifies, which induces a high-energy mine tremor, and its value falls back to the normal level after energy release; when S_D (see Fig. 7i) increases rapidly in time series, signifies a rapid increase in both the frequency and energy level of MS events. This increase indicates a more concentrated spatial distribution of these events and a heightened degree of internal rupture within the coal and rock mass. Consequently, it is accompanied by the occurrence of rockbursts; b (see Fig. 7p) decreases rapidly before the occurrence of a rockburst, and then fluctuates in the low value range, indicating that the level of stress concentration within the coal rock mass and the degree of elastic energy accumulation increase, leading to a rapid increase in the proportion of large rupture, and the possibility of a high-energy tremor increases, making it more likely to induce a rockburst. Each index in the rockburst precursory indices library reflects the precursor evolution law of rockburst from the multi-dimensional "temporal-spatial-intensity" and corresponds to the existence of certain characterization laws, which can monitor and warn the rockburst risk.

3.3. Evaluation of the early warning effectiveness and selection of indices

To monitor the rockburst hazard in the mine, the study employed the MKT with a 15-d time window and a 1-d sliding step. This analysis was conducted to evaluate the change trend of each precursory index, considering the rockburst characterization law outlined in Section 3.2 and the associated change characteristics. For ease of reference, the 15 rockburst events mentioned in Table 3 were assigned numbers from 1 to 15 in chronological order. The results of assessing the trend of the precursory indices within a 15-d period preceding each rockburst event are presented in Table 4, where "I" indicates that the index has an increasing trend, "D" indicates that the index has a decreasing trend, and "-" indicates that the index does not pass the significance test and without a significant change trend.

The results depicted in Fig. 7 and Table 4 demonstrate that the change trends of the precursory indices, as determined by MKT, largely align with the qualitative judgment results and adhere to the characterization law derived for the precursory indices. This indicates that the MKT method is effective in monitoring and providing warnings for rockburst hazards. However, it should be noted that a single precursory index has limitations in capturing

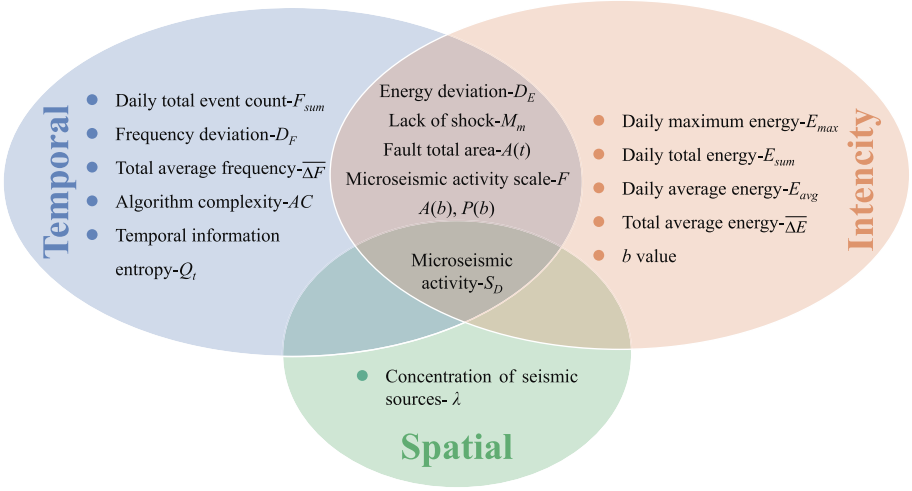

Fig. 6. The library of precursory indices.

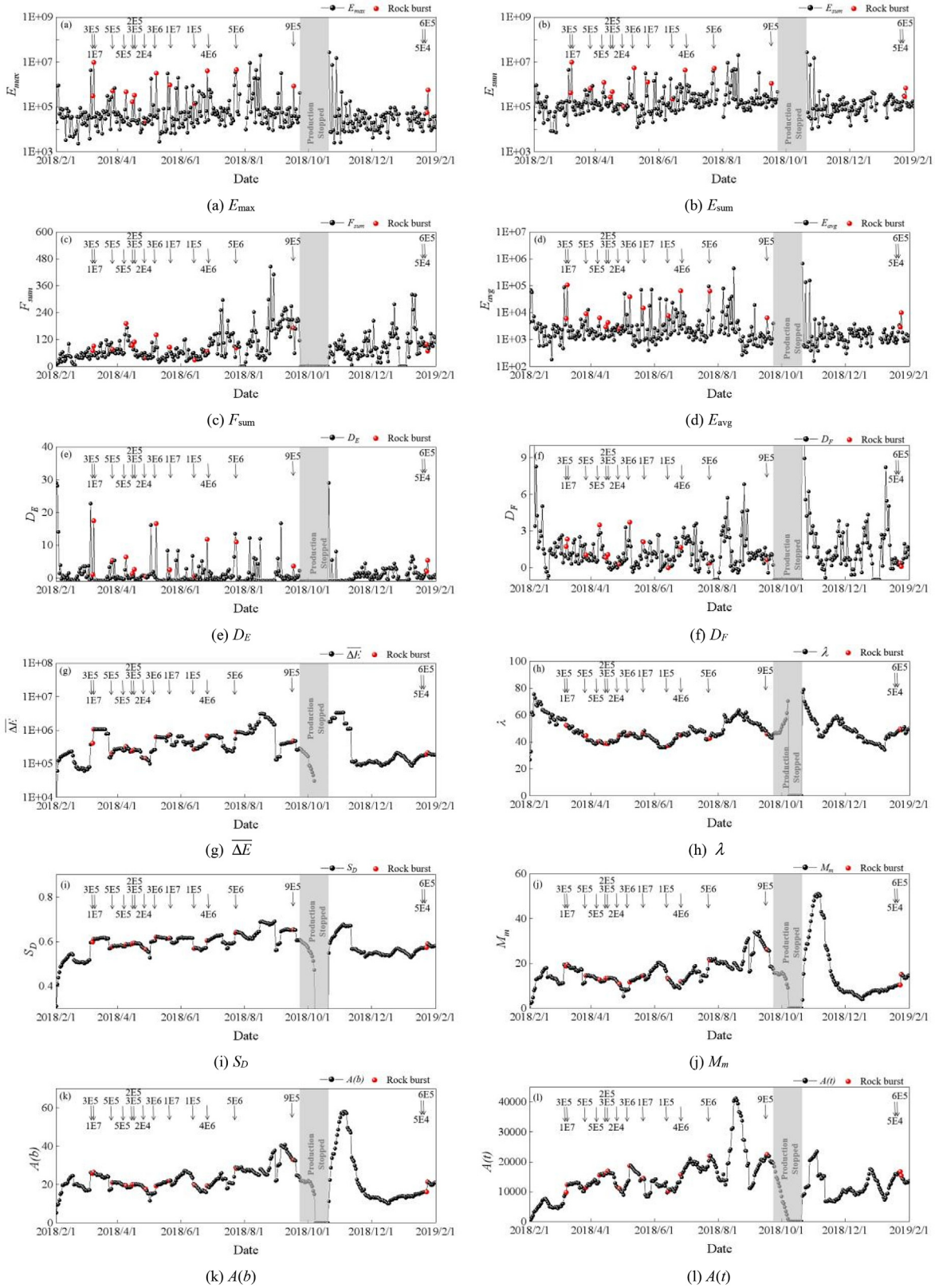

Fig. 7. Temporal evolution of MS precursory indices before and after rockburst events.

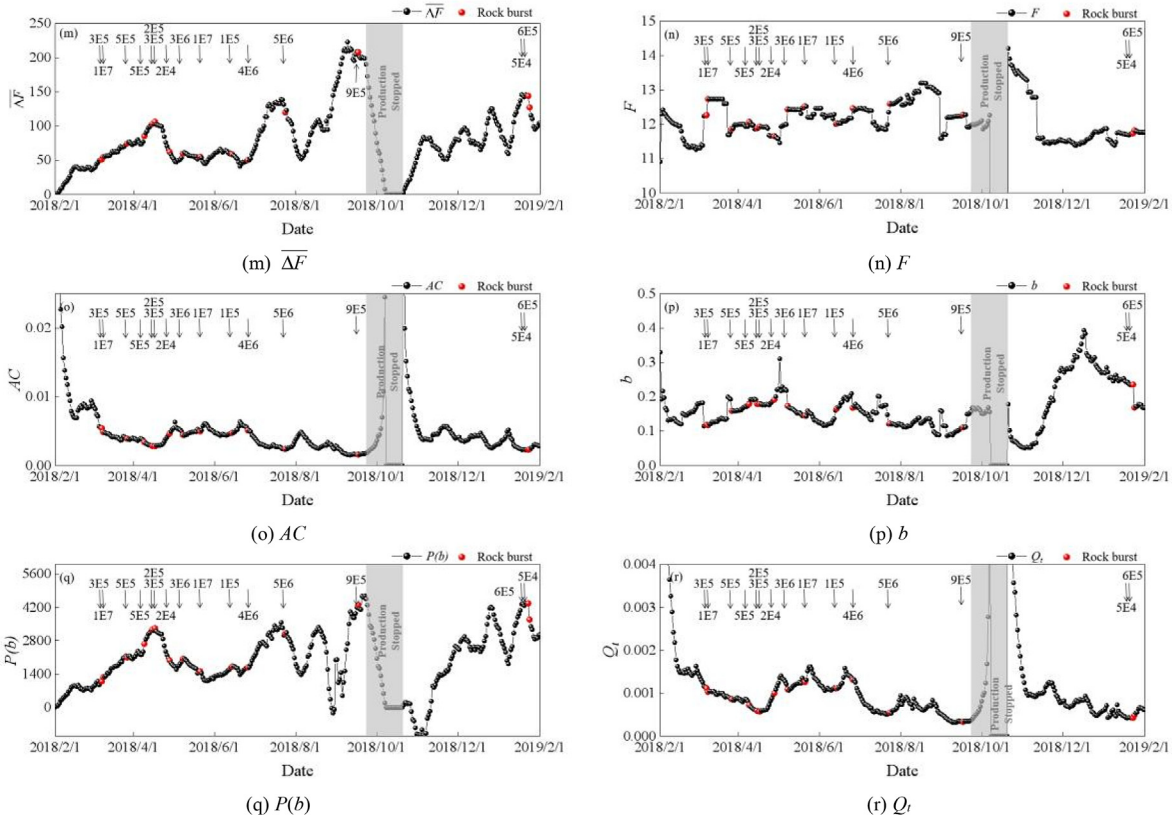

Fig. 7. (*continued*).

Table 4
Trend determination results of each precursory index before rockbursts and its early warning effectiveness.

Precursory indices	Rockburst events															*Recall*	*Precision*	*F_score*	Ranking
	1	2	3	4	5	6	7	8	9	10	11	12	13	14	15				
E_{max}	–	–	I	–	–	–	–	I	–	–	–	–	–	–	–	0.500	0.563	0.529	1
E_{sum}	–	I	–	–	–	–	–	I	–	–	–	–	–	–	–	0.444	0.308	0.364	4
F_{sum}	–	I	–	–	–	–	D	–	–	–	–	–	–	D	D	0.556	0.192	0.286	6
E_{avg}	–	–	–	–	–	–	–	–	–	I	–	–	–	–	I	0.389	0.350	0.368	3
D_E	–	–	I	–	–	–	–	I	–	–	–	I	–	D	–	0.611	0.239	0.344	5
D_F	–	–	–	–	–	–	–	I	–	–	I	–	–	D	D	0.667	0.316	0.429	2
$\overline{\Delta E}$	–	I	D	I	–	–	D	–	–	D	I	–	I	I	I	0.278	0.044	0.076	14
S_D	I	I	–	–	I	I	D	–	–	–	–	–	I	I	I	0.222	0.030	0.053	18
M_m	–	–	D	–	D	–	–	D	I	–	D	–	–	I	I	0.222	0.033	0.058	16
$A(b)$	–	–	D	–	D	–	–	D	I	–	D	–	–	I	I	0.222	0.034	0.058	16
$A(t)$	I	I	D	I	I	I	D	–	D	D	I	–	I	I	I	0.278	0.035	0.062	15
$\overline{\Delta F}$	I	I	I	I	I	I	D	D	D	–	D	–	–	I	I	0.389	0.044	0.079	13
F	–	I	D	I	–	D	D	–	–	D	I	–	I	–	–	0.444	0.101	0.165	9
AC	D	D	D	D	D	D	I	I	I	–	I	D	D	D	D	0.611	0.172	0.268	7
B	–	–	I	I	I	I	–	I	D	–	I	–	–	D	D	0.444	0.072	0.124	10
Q_t	D	D	D	D	D	D	I	I	I	D	I	D	D	D	D	0.444	0.052	0.092	12
Λ	–	–	D	D	–	–	I	I	–	D	I	D	D	I	I	0.444	0.057	0.101	11
$P(b)$	I	I	I	I	I	I	D	D	D	I	–	I	I	I	I	0.611	0.172	0.268	7

Note: Rockburst events serial numbers correspond to that in Table 3.

the complete evolutionary patterns of rockburst precursors. Consequently, relying solely on a single index may not always yield accurate early warnings for every rockburst event. For example, Q_t exhibits a declining trend prior to events 1–6, 10, and 12–15, and it has good early warning effectiveness as a negative rockburst precursory index accurately warning 11 out of 15 rockburst events. Furthermore, the different dimensions of each early warning index may contribute to vary early warning results for the same event. For example, prior to the onset of rockburst 8, D_E in the intensity dimension and D_F in the temporal dimension show an increasing trend as positive indices warn the danger, while λ in the spatial dimension also shows an increasing trend as a negative index and does not successfully warn of the occurrence of rockburst 8. Therefore, it is necessary to fuse the indices in the precursory library, the advantages of different dimensions of indices complement each other, which can be more efficient and accurate monitoring and warning of rockburst hazards.

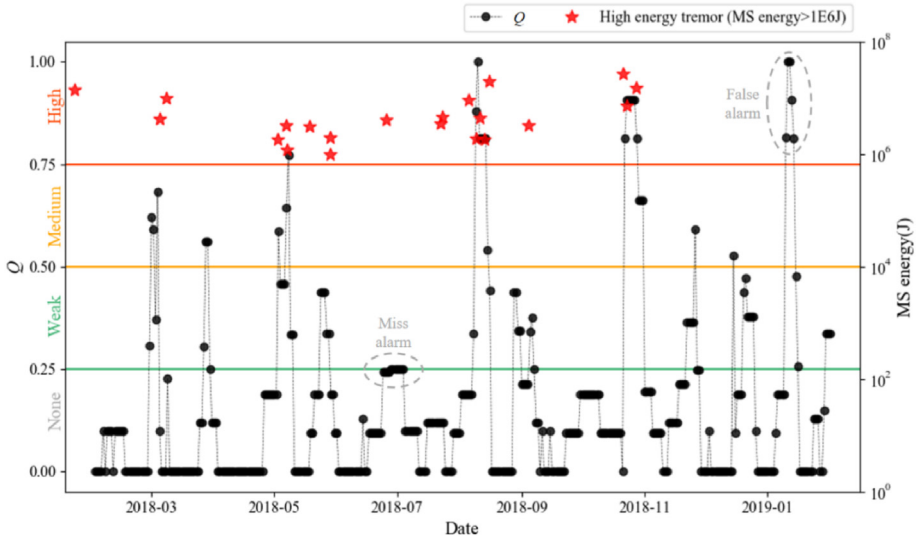

Fig. 8. Warning results of *Q*.

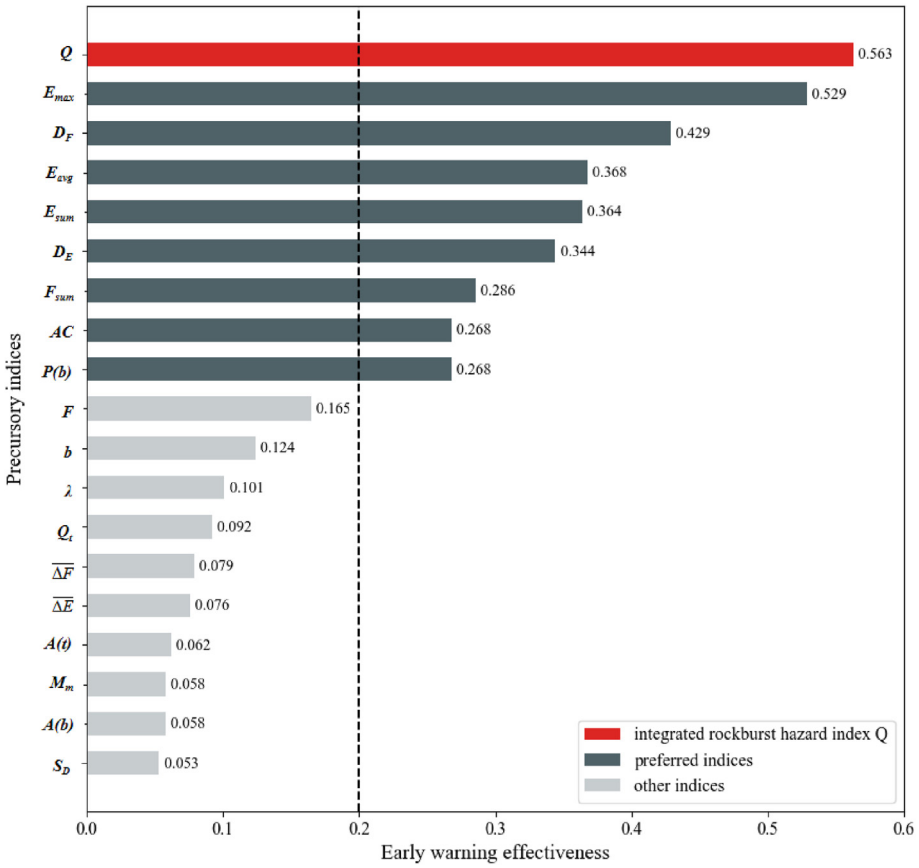

Fig. 9. Comparing the effectiveness of early warning indices.

The precursory index is deemed accurate if it exhibits an abnormal trend within 5 d before the occurrence of a high-energy tremor (with energy greater than 10^6 J). Specifically, positive precursory indices should demonstrate an increasing trend, while negative precursory indices should show a decreasing trend. Any deviation from these criteria would be classified as a missed or false alarm. The choice of a 5-d period for early warning indices is in accord with the practical experience of KCM, and it can be adjusted for other mines based on their specific requirements. To evaluate the early warning effectiveness of each index, the confusion matrix (refer to Table 1) is utilized. From the confusion matrix, the *Recall*, *precision*, and *F_score* of each index can be calculated. Table 4 presents the results of the early warning effectiveness for each index.

Based on Table 4, the precursory indices can be ranked in terms of their early warning effectiveness as follows: $E_{max} > D_F > E_{avg} > E_{sum} > D_E > F_{sum} > AC =$

$P(b) > F > b > \lambda > Q_t > \overline{\Delta F} > \overline{\Delta E} > A(t) > M_m = A(b) > S_D$. Notably, the indices in the intensity dimension generally exhibit higher early warning effectiveness compared to those in the temporal and spatial dimensions. These findings suggest that the precursory indices related to intensity in rockburst events carry a higher level of information entropy compared to the temporal and spatial indices. The energy characteristics of MS play a crucial role in capturing the evolutionary process of rockburst precursors. These intensity-based indices demonstrate a high level of effectiveness in reflecting the underlying dynamics of rockburst events. As a result, they hold significant importance and should receive increased attention in practical applications for improved rockburst prediction and early warning systems.

To maximize the effectiveness of early warning, the model selected preferred indices from each dimension. Out of the precursory indices library, eight indices (E_{max}, D_F, E_{avg}, E_{sum}, D_E, F_{sum}, *AC*, $P(b)$) were chosen based on their *F_scores* exceeding 0.2. These selected indices accounted for 74.9% of the total warning effectiveness and covered a significant portion of the intensity dimensions of rockburst hazard precursory indices. This selection ensures a strong foundation for the overall warning capability of the model. Regular re-evaluation and optimization of the early warning performance of each index in the precursory indices library are important to maintain the scalability and robustness of the model. Ideally, this re-evaluation should occur at least once every month. By dynamically updating the model based on actual field data, it can effectively assist relevant personnel in making rockburst warning decisions. This approach ensures that the model remains adaptable to changing conditions and maintains its efficiency in real-world applications.

3.4. Multi-indices fusion early warning of rockburst

3.4.1. Application effect test

The *F_score* of each rockburst precursory index is utilized to calculate the weight assigned to each index. This approach ensures that indices with higher warning effectiveness receive higher weights, while indices with lower warning effectiveness are given lower weights. By combining these weights with Eq. (6), *Q* is calculated. The time-series of *Q* is depicted in Fig. 8. Observing the curve, it is evident that the majority of *Q* values exceed 0.5 within a 5-d period prior to the occurrence of high-energy tremors. This corresponds to the medium or strong rockburst hazard category described in Table 2. The results indicate a strong correlation between the index and the occurrence of rockburst. Moreover, it demonstrates the capability of the index to provide effective monitoring and early warning for rockburst events.

The *Q* demonstrated strong performance in terms of *F_score*, *Recall*, and *Precision*, with values of 0.563, 0.500, and 0.643, respectively. These metrics indicate that *Q* outperformed individual warning indices, exhibiting higher *F_score* and *Precision*. This suggests that *Q* has improved warning effectiveness, as depicted in Fig. 9. However, the *Recall* of *Q* is lower than the 5 single precursory indices D_F (*Recall* = 0.667), $P(b)$ (*Recall* = 0.611), *AC* (*Recall* = 0.611), D_E (*Recall* = 0.611) and F_{sum} (*Recall* = 0.556). This means that the accuracy of *Q*'s early warning for the actual occurrence of high-energy tremors in the original monitoring data is lower than these five single indices, which are more conservative in the early warning process compared to the single indices, and will only warn when the predicted outcome is a high probability of rockburst events, which is shown as *Precision* is higher than other single indices.

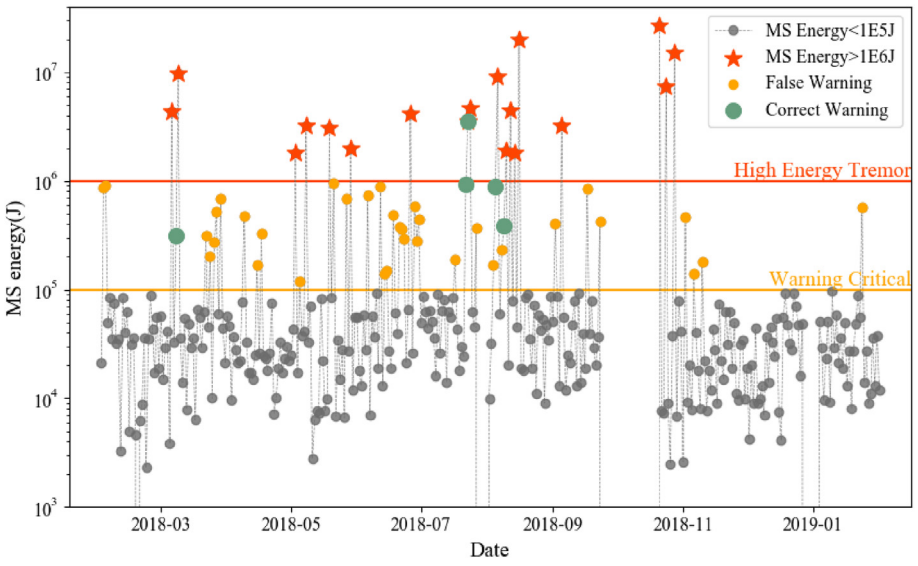

Fig. 10. Results of previous early warning method in KCM.

Table 5
Early warning results of the previous model.

Total population		Actual condition	
		Rockburst or high energy tremor (Positive)	No rockburst or high energy tremor (Negative)
Early warning condition	Rockburst or high energy tremor (Positive)	5	34
	No rockburst or high energy tremor (Negative)	13	296

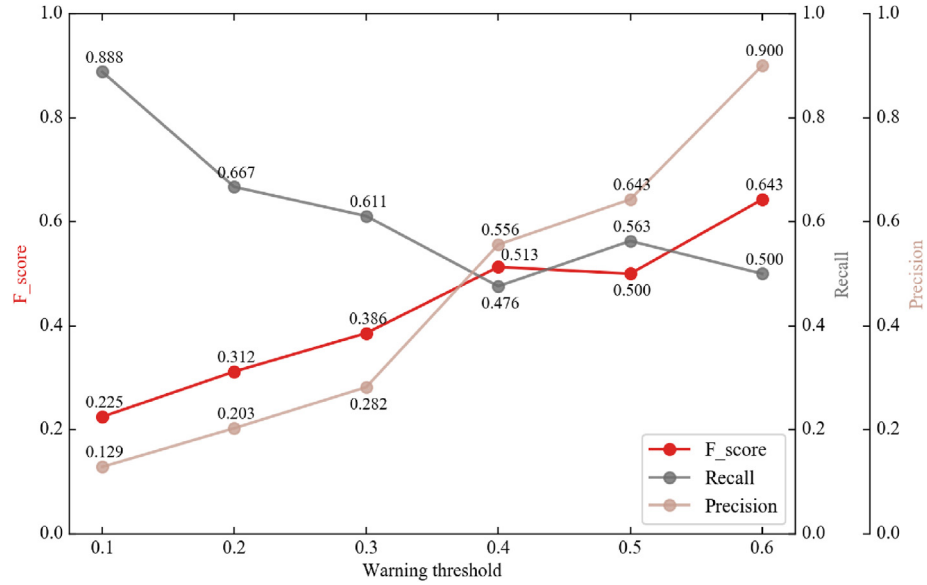

Fig. 11. Comparing the effectiveness of warnings under different thresholds.

In general, *Q* offers several advantages compared to single precursory indices. By combining multiple indices from different dimensions, *Q* incorporates the strengths of each index and establishes warning criteria among the indices. This approach eliminates the influence of singular values and improves the accuracy of the warning, resulting in higher integrated warning effectiveness compared to single indices. Furthermore, *Q* serves as a unified quantitative evaluation index for rockburst hazard, overcoming the issue of conflicting early warning results from multiple sources. It provides clear quantitative classification criteria, as shown in Table 2, which significantly reduces the management cost associated with underground rockburst prevention and control. Moreover, *Q* is data-driven, as its base indices are regularly updated. This ensures its adaptability and stability under complex working conditions. By assisting personnel in making efficient and accurate disaster prevention and control decisions, *Q* helps avoid major casualties and property damage.

3.4.2. Comparison with previous models

Previously, rockburst early warnings at KCM relied on monitoring high-energy MS events, specifically those with energy exceeding 10^5 J. According to the criterion, if an MS event at the working face had energy surpassing 10^5 J, it indicated a dangerous state, whereas energy below this threshold indicated a safe condition. To assess rockburst warning using this approach, the daily maximum MS energy data from February 1, 2018, to January 31, 2019, was utilized, and the results are shown in Fig. 10.

The effectiveness of the previous MS warning method was evaluated based on issuing a hazard warning within the same day. If a warning was issued on the same day as the hazard occurred, it was considered as a correct report; otherwise, it was classified as a missed or false alarm. The early warning results of the previous method are presented in Table 5, indicating that the method had a high missing rate. In 13 out of 18 d when actual hazards occurred, no warning was issued. This high missing rate could lead to severe consequences as the necessary measures were not taken in a timely manner. After calculating the metrics, it was found that the previous model had a significantly lower early warning effectiveness, with *Precision* of 0.128, *Recall* of 0.278 and *F_score* of 0.175 compared to the multi-indices fusion rockburst early warning model proposed in this paper.

The low effectiveness of the previous model can be attributed to several factors. Firstly, the previous model solely relied on the daily maximum energy (E_{max}) index in the intensity dimension of rockburst hazard precursory indices. This approach neglected the temporal and spatial dimensions, resulting in the loss of important information regarding the evolution of rockburst precursors. Consequently, the overall warning effectiveness was compromised. Additionally, the previous model utilized a single critical value for issuing warnings, which limited its ability to fully leverage the potential of the precursory indices. In contrast, the new model takes into account the change trend information of the E_{max} index, resulting in an early warning effectiveness of 0.529, making it the most effective single warning indicator. In comparison, the previous model generated several missed alarms. Consequently, the new model achieved an early warning effectiveness 3.2 times higher than that of the previous model.

In summary, the new model effectively enhances the accuracy of rockburst prediction by utilizing multiple dimensions of precursory indices and leveraging their full potential.

4. Discussion

Given the unclear mechanism of rockburst hazards in mines operating under complex working conditions, accurately and efficiently predicting and controlling these hazards remains challenging. While significant progress has been made in monitoring and early warning systems, there is still a need for a highly scalable and accurate rockburst early warning model. To address this, the present study proposes an MKT-based multi-indices fusion early warning model for rockburst hazards (refer to Fig. 1). This model leverages multidimensional warning indicators to capture the precursor trends that reflect the evolution of rockbursts. It incorporates the use of a confusion matrix to evaluate the effectiveness of individual warning indices and periodically optimizes the indices based on this evaluation. The integrated rockburst hazard index *Q* (refer to Fig. 8) demonstrates that it can reach a medium- or high-hazard warning level within 5 d prior to the occurrence of most high-energy tremors. The warning effectiveness of the model

reaches 0.563, representing a significant improvement compared to relying on a single warning index (refer to Fig. 9). The model has the capability to dynamically adjust the selection of indices based on real-time monitoring data in the field. This adaptability allows it to effectively respond to changing working conditions and ensures the production of stable warning results. The practicality of the model is strengthened by providing reliable warning outcomes for the prevention and control of rockbursts in mining operations.

In contrast to previous studies that primarily relied on exceeding hazard thresholds or qualitative human judgment to trigger warnings, this study employs mathematical-statistical methods to capture the changing trends of multidimensional warning indicators in real-time. This approach enables a comprehensive representation of the overall evolution process, including fissure initiation, propagation, convergence, and the formation of macro-fractures in coal and rock masses that ultimately lead to rockburst occurrences. Warnings are only issued when the indicator's change trend clearly aligns with the rockburst precursor response. Furthermore, the study incorporates the use of a confusion matrix to comprehensively evaluate the effectiveness of each individual precursory index. By considering the warning effectiveness of each index, the model can select the most appropriate indices that align with the actual conditions of the mine. This selection process enhances the overall warning performance of the model and ensures that low-effectiveness indices, which may not adequately represent the mine's specific conditions, do not negatively impact the warning results. The periodic re-evaluation and optimization of indices based on data-driven self-feedback further maintains the model's effectiveness and sustainability within the complex underground environment. Moreover, this approach significantly reduces human operation and management costs. In practical applications, it is important to note that for mines with newly installed online monitoring systems, equal weights can be initially assigned to the warning indices. The remaining calculations should remain unchanged until sufficient data becomes available.

In mining practice, rockburst accidents can lead to significant losses. Therefore, it is crucial for an early warning model to minimize both missed alarms (where the model fails to predict a rockburst event that occurs) and false alarms (where the model issues a warning but no rockburst occurs). The costs associated with these two scenarios can vary significantly for the mine. The evaluation of the warning model's effectiveness relies on the use of the confusion matrix, specifically focusing on *Precision* and *Recall*. *Precision* measures the accuracy of the model's warnings relative to the total number of warnings issued, while *Recall* measures the accuracy of predicting actual rockburst occurrences relative to the total number of actual rockbursts. The *F_score* is the harmonic mean of *Precision* and *Recall*, providing a comprehensive assessment of the model's performance. Maximizing both *Precision* and *Recall* is crucial for achieving optimal performance. However, achieving high values for both measures simultaneously can be challenging in practice. Mines often prioritize models with higher *Recall* to minimize the risk of significant losses. To address this, different warning thresholds can be set in the model to determine the changes in indices. The results of applying different warning thresholds are presented in Fig. 11. These thresholds allow for fine-tuning the model's sensitivity and strike a balance between missed forecasts and false alarms, taking into account the specific requirements and risk tolerance of the mine.

It can be seen that as the warning threshold increases, the model's *Precision* increases while *Recall* decreases. The highest *F_score* of 0.643 is achieved at a warning threshold value of 0.6. However, it is important to note that at this threshold, the *Recall* decreases to 0.5, indicating that the model issues warnings only when it is more confident in its predictions, resulting in an increased number of missed alarms. On the other hand, the *F_score* of 0.513 is obtained at a warning threshold value of 0.4, which is higher than the threshold of 0.5. However, the *Recall* at this threshold drops significantly to 0.476 compared to the *Recall* of 0.643 at the threshold of 0.5. Considering a comprehensive evaluation, a warning threshold value of 0.5 for Q appears to strike a balance between *Precision* and *Recall*, achieving a reasonable *F_score* of 0.643 while maintaining a *Recall* of 0.5. This threshold value aligns with the concept of "producer equilibrium" for mining enterprises, taking into account the trade-off between missed alarms and false alarms. Nevertheless, in practical applications, the threshold value can be adjusted based on the mine's own risk tolerance level to best align with its specific interests and requirements.

In the next step, we plan to use a "cost-sensitive" approach to further improve the rockburst early warning model, i.e. to apply a larger penalty to the model when it generates "missed" alarms and a smaller penalty when it generates "false" alarms so that the model can be trained to better suit the actual warning needs in the field and contribute to creating a safer environment in the mining industry.

5. Conclusions

Rockburst frequently result in significant casualties and property damage. Therefore, accurate monitoring and early warning systems are crucial for disaster prevention. This paper proposes a multi-indices fusion rockburst early warning model utilizing the MKT to enhance the quantitative and precise monitoring and warning of rockburst disasters. The main findings of this study are as follows:

(1) A rockburst early warning model based on MKT is developed, incorporating 18 rockburst precursory indices with clear physical significance. The model assesses the conformity of their temporal trends with the rockburst precursor characterization law to determine warnings. The effectiveness of each index is evaluated and ranked using the confusion matrix, and the indices with higher effectiveness are given more weight. The multi-indices fusion approach is employed using a comprehensive anomaly index method, resulting in the integrated rockburst hazard index Q. The values of Q correspond to four levels of rockburst hazard: none, weak, medium, and high.

(2) The field application results demonstrate that Q, serving as a unified quantitative evaluation index, combines the strengths of individual early warning indicators. It achieves an early warning effectiveness of 0.563, surpassing that of any single early warning index. Moreover, the indices from different dimensions provide complementary early warning criteria, mitigating conflicts in the results from multiple sources. The model outperforms the previous mine's early warning model by 3.2 times in effectiveness, effectively supporting mine personnel in making accurate and efficient disaster prevention and control decisions.

(3) The model has the capability to undergo periodic updates through self-feedback using real-time monitoring data from the field. This allows for the selection of indices that are most suitable for the complex and dynamic underground working environment, resulting in higher warning effectiveness. As a result, the model reduces the costs associated with human operation and management. Additionally, the model can provide stable early warning results based on online real-time monitoring data and exhibits strong scalability,

making it easily adaptable to other mine sites. Overall, this model represents an effective and innovative approach for monitoring and early warning of rockbursts.

Declaration of competing interest

The authors declare that they have no known competing financial interests or personal relationships that could have appeared to influence the work reported in this paper.

Acknowledgments

The authors gratefully acknowledge the financial support from the National Natural Science Foundation of China (Grant Nos. 52011530037 and 51904019) and the Fundamental Research Funds for the Central Universities and the Youth Teacher International Exchange & Growth Program (Grant No. QNXM20210004). We also greatly appreciate the assistance provided by Kuangou coal mine, China Energy Group Xinjiang Energy Co., Ltd.

References

Cai, W., Bai, X.X., Si, G.Y., Cao, W.Z., Gong, S.Y., Dou, L.M., 2020. A monitoring investigation into rock burst mechanism based on the coupled theory of static and dynamic stresses. Rock Mech. Rock Eng. 53 (12), 5451–5471.
Cai, W., Dou, L.M., Li, Z.L., Liu, J., Gong, S.Y., He, J., 2014. Microseismic multidimensional information identification and spatio-temporal forecastingof rock burst:A case study of Yima Yuejin coal mine, Henan, China. Chin. J. Geophys. 57, 2687–2700, 08.
Cai, W., Dou, L.M., Zhang, M., Cao, W.Z., Shi, J.Q., Feng, L.F., 2018. A fuzzy comprehensive evaluation methodology for rock burst forecasting using microseismic monitoring. Tunn. Undergr. Space Technol. 80, 232–245.
Cao, A.Y., Dou, L.M., Wang, C.B., Yao, X.X., Dong, J.Y., Gu, Y., 2016. Microseismic precursory characteristics of rock burst hazard in mining areas near a large residual coal pillar: a case study from Xuzhuang coal mine, Xuzhou, China. Rock Mech. Rock Eng. 49 (11), 4407–4422.
Cao, A.Y., Liu, Y.Q., Yang, X., Li, S., Liu, Y.P., 2022. FDNet: knowledge and data fusion-driven deep neural network for coal burst prediction. Sensors 22 (8).
Cao, W.Z., Durucan, S., Cai, W., Shi, J.Q., Korre, A., 2020. A physics-based probabilistic forecasting methodology for hazardous microseismicity associated with longwall coal mining. Int. J. Coal Geol. 232, 103627.
Dou, L.M., Cai, W., Cao, A.Y., Guo, W.H., 2018. Comprehensive early warning of rock burst utilizing microseismic multi-parameter indices. Int. J. Min. Sci. Technol. 28 (5), 767–774.
Dou, L.M., He, X.Q., 2007. Technique of classification forecasting rock burst in coal mines. J. China Inst. Min. Technol. 717–722, 06.
Fawcett, T., 2006. An introduction to ROC analysis. Pattern Recogn. Lett. 27 (8), 861–874.
Feng, G., Feng, X., Chen, B., Xiao, Y., Yu, Y., 2015. A microseismic method for dynamic warning of rockburst development processes in tunnels. Rock Mech. Rock Eng. 48 (5), 2061–2076.
Feng, G.L., Xia, G.Q., Chen, B.R., Xiao, Y.X., Zhou, R.C., 2019. A method for rockburst prediction in the deep tunnels of hydropower stations based on the monitored microseismicity and an optimized probabilistic neural network model. Sustainability-Basel. 11 (11), 3212.
Feng, X.T., Yu, Y., Feng, G.L., Xiao, Y.X., Chen, B.R., Jiang, Q., 2016. Fractal behaviour of the microseismic energy associated with immediate rockbursts in deep, hard rock tunnels. Tunn. Undergr. Space Technol. 51, 98–107.
Gutenberg, B.R.C., 1956. Earthquake magnitude. intensity, energy and acceleration. Bull. Seismol. Soc. Am. 46, 105–145.
He, H., Dou, L.M., Gong, S.Y., He, J., Zheng, Y.L., Zhang, X., 2019. Microseismic and electromagnetic coupling method for coal bump risk assessment based on dynamic static energy principles. Saf. Sci. 114, 30–39.
He, S.Q., Song, D.Z., He, X.Q., Chen, J.Q., Ren, T., Li, Z.L., Qiu, L.M., 2020. Coupled mechanism of compression and prying-induced rock burst in steeply inclined coal seams and principles for its prevention. Tunn. Undergr. Space Technol. 98, 103327.
He, S.Q., Song, D.Z., Mitri, H., He, X.Q., Chen, J.Q., Li, Z.L., Xue, Y.R., Chen, T., 2021. Integrated rockburst early warning model based on fuzzy comprehensive evaluation method. Int. J. Rock Mech. Min. 142, 104767.
Ji, B., Xie, F., Wang, X.P., He, S.Q., Song, D.Z., 2020. Investigate contribution of multi-microseismic data to rockburst risk prediction using support vector machine with genetic algorithm. IEEE Access 8, 58817–58828.
Jin, A.B., Basnet, P.M.S., Mahtab, S., 2022. Microseismicity-based short-term rockburst prediction using non-linear support vector machine. Acta Geophys. 70 (4), 1717–1736.
Kendall, M.G., 1948. Rank correlation methods. Br. J. Psychol. 25 (1), 86–91.
Khan, M., Xueqiu, H., Farid, A., Jianqiang, C., Honglei, W., Dazhao, S., Chao, Z., 2022. In: Geophysical Characterization of Mining-Induced Complex Geological Deformations in a Deep Coalmine, vol. 2021. Lithosphere-US (Special 4).
Li, X.L., Chen, S.J., Wang, E.Y., Li, Z.H., 2021. Rockburst mechanism in coal rock with structural surface and the microseismic (MS) and electromagnetic radiation (EMR) response. Eng. Fail. Anal. 124, 105396.
Liu, F., Tang, C.A., Ma, T.H., Tang, L.X., 2019. Characterizing rockbursts along a structural Plane in a tunnel of the hanjiang-to-weihe river diversion project by microseismic monitoring. Rock Mech. Rock Eng. 52 (6), 1835–1856.
Liu, G.F., Feng, X.T., Feng, G.L., Chen, B.R., Chen, D.F., Duan, S.Q., 2016. A method for dynamic risk assessment and management of rockbursts in drill and blast tunnels. Rock Mech. Rock Eng. 49 (8), 3257–3279.
Lu, C.P., Liu, G.J., Liu, Y., Zhang, N., Xue, J.H., Zhang, L., 2015. Microseismic multiparameter characteristics of rockburst hazard induced by hard roof fall and high stress concentration. Int. J. Rock Mech. Min. 76, 18–32.
Ma, C.C., Li, T.B., Zhang, H., 2019. Microseismic and precursor analysis of high-stress hazards in tunnels: a case comparison of rockburst and fall of ground. Eng. Geol.
Mann, H.B., 1945. Nonparametric tests against trend. Econometrica. J. Econom. Soc. 13 (3), 245–259.
Manouchehrian, A., Cai, M., 2017. Analysis of rockburst in tunnels subjected to static and dynamic loads. J. Rock Mech. Geotech. Eng. 9 (6), 1031–1040.
Mondal, D., Roy, P.N.S., 2019. Fractal and seismic b-value study during dynamic roof displacements (roof fall and surface blasting) for enhancing safety in the longwall coal mines. Eng. Geol. 253, 184–204.
Pu, Y.Y., Apel, D.B., Hall, R., 2020. Using machine learning approach for microseismic events recognition in underground excavations: comparison of ten frequently-used models. Eng. Geol. 268, 105519.
Pu, Y.Y., Apel, D.B., Liu, V., Mitri, H., 2019. Machine learning methods for rockburst prediction-state-of-the-art review. Int. J. Min. Sci. Technol. 29 (4), 565–570.
Qin, Z.C., Li, T., Li, Q.H., Chen, G.B., Cao, B., 2019. Combined early warning method for rock burst and its engineering application. Adv. Civ. Eng. 2019, 1–10.
Tang, Z.L., Liu, X.L., Xu, Q.J., Li, C.Y., Qin, P.X., 2018. Stability evaluation of deep-buried TBM construction tunnel based on microseismic monitoring technology. Tunn. Undergr. Space Technol. 81, 512–524.
Utsu, T., Ogata, Y., Matsu'Ura, R.S., 1995. The centenary of the omori formula for a decay law of aftershock activity. J. Phys. Earth 43 (1), 1–33.
Wang, G.F., Gong, S.Y., Dou, L.M., Wang, H., Cai, W., Cao, A.Y., 2018. Rockburst characteristics in syncline regions and microseismic precursors based on energy density clouds. Tunn. Undergr. Space Technol. 81, 83–93.
Wang, Y., 2021. Prediction of rockburst risk in coal mines based on a locally weighted C4.5 algorithm. IEEE Access (99), 1.
Xie, H., Pariseau, W.G., 1993. Fractal character and mechanism of rock bursts. Int. J. Rock Mech. Min. Sci. Geomech. Abstracts 30 (4), 343–350.
Xu, J., Jiang, J.D., Xu, N., Liu, Q.S., Gao, Y.F., 2017. A new energy index for evaluating the tendency of rockburst and its engineering application. Eng. Geol. 230, 46–54.
Xue, R.X., Liang, Z.Z., Xu, N.W., 2021. Rockburst prediction and analysis of activity characteristics within surrounding rock based on microseismic monitoring and numerical simulation. Int. J. Rock Mech. Min. 142, 104750.
Xue, R.X., Liang, Z.Z., Xu, N.W., Dong, L.L., 2020. Rockburst prediction and stability analysis of the access tunnel in the main powerhouse of a hydropower station based on microseismic monitoring. Int. J. Rock Mech. Min. 126, 104174.
Xue, Y.R., Song, D.Z., Chen, J.Q., Li, Z.L., He, X.Q., Wang, H.L., Zhou, C., Sobolev, A., 2023. Integrated rockburst hazard estimation methodology based on spatially smoothed seismicity model and Mann-Kendall trend test. Int. J. Rock Mech. Min. 163, 105329.
Yin, X., Liu, Q.S., Huang, X., Pan, Y.C., 2021. Real-time prediction of rockburst intensity using an integrated CNN-Adam-BO algorithm based on microseismic data and its engineering application. Tunn. Undergr. Space Technol. 117, 104133.
Yu, Y., Chen, B.R., Xu, C.J., Diao, X.H., Tong, Shi, Y.F., 2016. Analysis for microseismic energy of immediate rockbursts in deep tunnels with different excavation methods. Int. J. GeoMech., 4016119
Yu, Y., Chen, B.R., Xu, C.J., Diao, X.H., Tong, L.H., Shi, Y.F., 2017. Analysis for microseismic energy of immediate rockbursts in deep tunnels with different excavation methods. Int. J. GeoMech., 4016119
Zhang, W.L., Ma, N.J., Ren, J.J., Li, C., 2021. Peak particle velocity of vibration events in underground coal mine and their caused stress increment. Measurement 169, 108520.
Zhao, H.B., Chen, B.R., Zhu, C.X., 2021. Decision tree model for rockburst prediction based on microseismic monitoring. Adv. Civ. Eng. 2021, 1–14.
Zhu, S.T., Feng, Y., Jiang, F.X., 2016. Determination of abutment pressure in coal mines with extremely thick alluvium stratum: a typical kind of rockburst mines in China. Rock Mech. Rock Eng. 49 (5), 1943–1952.
Zhu, S.T., Feng, Y., Jiang, F.X., Liu, J.H., 2018. Mechanism and risk assessment of overall-instability-induced rockbursts in deep island longwall panels. Int. J. Rock Mech. Min. 106, 342–349.